Geomechanics and Engineering, *Vol. 11, No. 1 (2016) 41-58*
DOI: http://dx.doi.org/10.12989/gae.2016.11.1.041

Effect of spatial characteristics of a weak zone on tunnel deformation behavior

Chungsik Yoo*

School of Civil, Architectural Engineering and Landscape Architecture, Sungkyunkwan University, 2066 Seboo-ro, Jangan-gu, Suwon, Kyounggi-do 16419, Republic of Korea

(*Received November 14, 2015, Revised February 25, 2016, Accepted March 11, 2016*)

Abstract. This paper focuses on the deformation behavior of tunnels crossing a weak zone in conventional tunneling. A three-dimensional finite element model was adopted that allows realistic modeling of the tunnel excavation and the support installation. Using the 3D FE model, a parametric study was conducted on a number of tunneling cases with emphasis on the spatial characteristics of the weak zone such as the strike and dip angle, and on the initial stress state. The results of the analyses were thoroughly examined so that the three-dimensional tunnel displacements at the tunnel crown and the sidewalls can be related to the spatial characteristic of the weak zone as well as the initial stress state. The results indicate that the effectiveness of the absolute displacement monitoring data as early warning indicators depends strongly on the spatial characteristics of the weak zone. It is also shown that proper interpretation of the absolute monitoring data can provide not only early warning for a weak zone outside the excavation area but also information on the orientation and the extent of the weak zone. Practical implications of the findings are discussed.

Keywords: conventional tunneling; finite element analysis; absolute displacement monitoring; weak zone; deflection line; displacement ratio

1. Introduction

The use of underground spaces including tunnels is increasing due primarily to the pressing need for sustainable development. Tunneling conditions are however becoming more aggressive due in part to construction as well as environmental constraints (Yoo and Park 2014). For example, high speed railway and road tunnels tend to be long and constructed at great depth. Such long and deep tunnels are usually characterized by great risks associated with uncertainties of the ground conditions due largely to limited ground information available during design and construction stages (e.g., ITA 2010, Shin *et al*. 2011, Kun and Onargan 2013, Yang and Yan 2015).

Due to the fact that the ground conditions cannot be fully defined with the required accuracy prior to construction in many tunneling situations, it is necessary to continuously update the geotechnical model and adjust the excavation and support methods to the actual ground conditions during construction. To overcome the uncertainties involved in the ground conditions, monitoring and control have become essential aspects of tunneling as this allows for the verification of design

*Corresponding author, Professor, E-mail: csyoo@skku.edu

 ISSN: 2005-307X (Print), 2092-6219 (Online)

parameters, quality control, observation of the effectiveness of construction methods as well as the rock mass behavior, etc., (Schubert *et al*. 2002).

Over the decades, monitoring techniques have been considerably improved (Miranda *et al*. 2015). For example, absolute displacement monitoring during tunnel excavation by geodetic methods is to a large extent replacing measurements of relative displacement. There have been a number of studies and practical applications on the use of absolute displacement monitoring data for prediction of ground conditions ahead of an advancing tunnel. For example, based on data gained from tunneling sites in Austria, Schubert (1993) has shown that the ratio between radial and longitudinal displacements could be used as an indicator for identifying weak zones ahead of the tunnel face. This hypothesis was later verified using three-dimensional numerical simulations, showing that the displacement vector orientation, deflection curve, and the trend line can be used for prediction of weak zones ahead of the tunnel heading (e.g., Lee *et al*. 1998, Schubert and Vavrovsky 1994, Schubert and Budil 1995, Steindorfer and Schubert 1997, Steindorfer 1998, Kim *et al*. 2003, Jeon *et al*. 2005, Goswami and Sharma 2014, Yoo *et al*. 2013, Yoo and Park 2014), which eventually allow execution of mitigation measures before the tunnel enters the weak zone in a timely manner. Based on the outcome of previous research, Sellner (2000) later developed a simple and practically applicable software which allows a quick estimation of displacements in tunneling.

Aforementioned studies have identified the important governing mechanisms of the tunnel displacement behavior with changing ground conditions and demonstrated their practical applications. Most of the previous studies, however, adopted rather ideal and simplified tunneling situations, which in turn limits applicability of the findings in real tunneling situations. For example, most of the earlier numerical work did not consider the spatial characteristics of weak zones and assumed the ground as a linear elastic material with no tunnel support considered. More detailed studies are warranted considering tunneling situations not covered in the previous studies using a more realistic numerical model.

In this paper, the results of a three-dimensional numerical investigation into the deformation behavior of tunnels crossing a weak zone of various orientations in conventional tunneling are presented. The aim of the study is to supplement additional data to the findings from the aforementioned previous studies. A series of hypothetical tunneling situations were developed to cover a wide range of spatial variations of a weak zone relative to the tunnel advancing direction in terms of the strike and dip angle together with different initial stress states. A parametric study was then conducted using a 3D finite element model which can realistically model the non-linear material behavior of the ground, the actual tunneling sequence, as well as support installation. The following sections present the tunneling and site conditions, the 3D finite-element model, and the practical implications of the findings.

2. Tunneling conditions considered

2.1 Tunneling and subsurface conditions

In this study, tunneling situations in which a tunnel crosses a 6 m wide weak zone of various orientations were considered as shown in Fig. 1. A typical railway tunnel section was considered (IARCA 2002), having a maximum height (H) and width (D) of 9 m and 11 m, respectively, giving a net excavation area of approximately 90 m^2. Fig. 2 shows detailed tunnel dimensions and

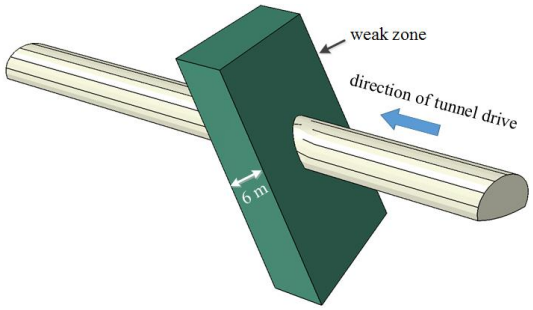

Fig. 1 Graphical representation of tunneling condition

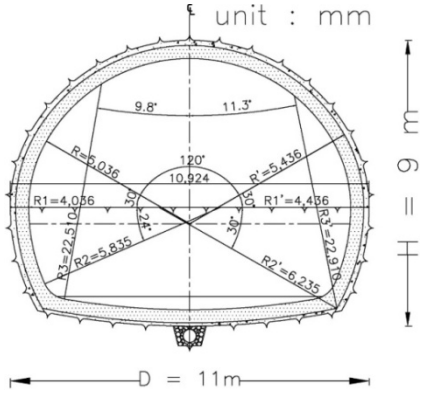

Fig. 2 Tunnel cross section

Table 1 Geotechnical properties of ground and weak zone

Type	γ^* (kN/m³)	c' (kPa)	ϕ' (deg)	φ (deg)	E (MPa)	v
Ground	25	100	35	20	500	0.20
Weak zone	20	50	30	20	100	0.25

* γ = unit weight; c' = cohesion; ϕ' = internal friction angle;
φ = dilatancy angle; E = Young's modulus; v = Poisson's ratio

the shape of the tunnel. The tunnel was assumed to be excavated at a depth of 10D in full face with a 200 mm thick shotcrete layer as a primary support. Although system rock bolts, together with other auxiliary methods such as the fore poling and the pipe roofing techniques, are usually adopted in this type of tunneling situation, they are not considered in this study for simplicity. In addition, the support pattern as well as the excavation method were assumed to remain the same for the section crossing the weak zone for ease of interpretation of the results.

The ground through which the tunnel is excavated was assumed to be a poor to fair rock layer of Grade II~III, as per the engineering classification of rock (Waltham 1994), having RMR values ranging from 30 to 50. Table 1 shows the geotechnical properties of the ground and the weak zone. Note that these properties were obtained by Yoo *et al*. (2012) from a design case history in which a similar ground condition was involved.

2.2 Orienetations of weak zone considered

The spatial characteristics of the weak zone were considered in this study by varying its strike and dip angle. Fig. 3 shows symbols that define the orientation of the weak zone. In this study, three sets of analysis were devised, namely ***Series A***, ***Series B***, and ***Series C***. ***Series A*** concerns the cases in which the strike of the weak zone (θ_{yz}) makes 90° to the tunnel axis, i.e., θ_{xy} = 0 with varying dip angle θ_{yz}. In ***Series B***, on the other hand, the strike θ_{xy} of the weak zone was varied with a fixed dip angle of θ_{yz} = 90°. Finally, ***Series C*** involves cases with varying strike of θ_{xy} with dip angles of θ_{yz} = ±60°. Note that a positive θ_{yz} represents tunnel driving with the dip while a negative θ_{yz} indicates tunnel driving against the dip. Table 2 summarizes the orientations of the weak zone considered in this study.

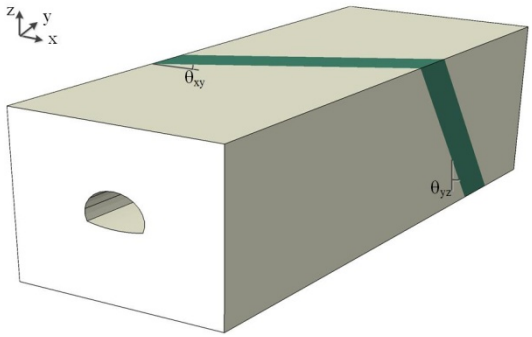

Fig. 3 Graphical representation of weak zone orientation

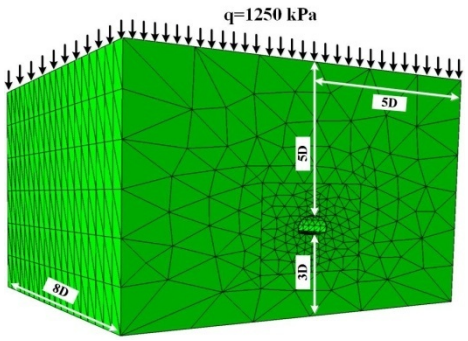

Fig. 4 3D finite element model

Table 2 Orientations of weak zone considered

Series	CASE	θ_{xy} (deg)	θ_{yz} (deg)	K_o	Note
A	xy0yz (±30)	0	±30	0.5, 1.0, 2.0	Cases with negative θ_{yz} represent tunnel driving against dip
	xy0yz 60		60		
	xy0yz90		90		
***B*(*C*)**	xy30yz90 (±60)	30	90 (±60)		
	xy60yz90 (±60)	60			

3. Three dimensional finite element analysis

A commercially available finite element software package Abaqus (2013) was used for analysis. Three-dimensional finite element models capable of simulating the sequential tunneling process were adopted in order to realistically capture the three-dimensional tunnel and weak zone interaction. A particular attention was paid to the modeling of the weak zone with different orientations so as to allow for a realistic consideration of practical tunneling situations. Details of the three-dimensional model are given under the subsequent subheadings.

3.1 3D finite element model

Fig. 4 shows a typical finite element model adopted in the analysis, consisting of almost 45,000 three-dimensional elements with over 55,000 nodes. Considering the asymmetric condition in terms of the weak zone orientation relative to the tunnel advancing direction in most of the cases considered in this study, the full domain was included in the finite element model. In order to define the model, the lateral boundaries were placed at locations with sufficient distance to eliminate possible boundary effects; i.e., 5D from the tunnel center for the lateral vertical boundaries and 8D from the tunnel portal for the longitudinal vertical boundary, and the bottom boundary at 3D from the tunnel invert (Fig. 4). In terms of the displacement boundary condition, roller boundaries were placed on the vertical faces of the mesh, i.e., $U_x = 0$ or $U_y = 0$, while a fixed boundary condition was assumed at the bottom boundary considering the rigid rock layer. In order to reduce the size of the finite element domain, the upper 5D zone was replaced with an equivalent surcharge of q = 1250 kPa, which was calculated based on the unit weight of the ground.

In discretizing the model, the ground was modeled using 10-node tetrahedron elements (C3D10), while three-dimensional conventional shell elements with five degrees of freedom (STRI65) were used for the shotcrete lining. With regard to the constitutive modeling, the ground including the weak zone was assumed to be an elasto-plastic material conforming to the Mohr-Coulomb failure criterion, together with the non-associated flow rule proposed by Davis (1968), while the shotcrete lining was assumed to behave in a linear elastic manner. Note that a dilatancy angle of $\varphi = 20°$ was assumed for the ground as well as the weak zone. The time dependency of the strength and stiffness of the shotcrete lining after installation was not explicitly modeled in the analysis; instead, an average value of Young's modulus of 10 GPa, representing the green and hard shotcrete conditions reported in the literature (Queiroz *et al*. (2006)), was employed with a Poisson's ratio and a unit weight of 0.25 and 23 kN/m³, respectively.

3.2 Modeling of tunneling sequence

After creating the initial stress condition of the ground with the appropriate boundary conditions, the tunneling process, consisting of a series of excavation and shotcrete lining installation, was closely followed by removing and adding corresponding elements at designated steps, assuming full face excavation with an advance length of 2 m. The 80 m long tunnel was therefore excavated in 40 steps in total.

4. Results and discussion

The results of the series of 3D finite element analyses were examined in terms of the deflection curves for crown settlement, longitudinal displacements at crown and sidewalls, trend lines of displacement ratios so that the tunnel deformation behavior in relation to the orientation of the weak zone as well as the initial stress state could be identified. Note here that a deflection curve was constructed by connecting settlement values ($\delta_{cr,z}$) at measuring points along the tunnel crown while displacement ratios are expressed as the ratios of the left ($\delta_{lsp,x}$) and right ($\delta_{rsp,x}$) sidewall convergence to the crown settlement ($\delta_{cr,z}$). All the displacement data presented here represent those with $K_o = 1.0$ unless otherwise indicated.

4.1 General tunnel displacement characteristics

In this section, the tunnel deformation behavior of the case, where the tunnel approaches a weak zone steeply dipping ($\theta_{yz} = 90°$) and gently striking to the tunnel axis at an angle of $\theta_{xy} = 30°$, is presented along with that of the no weak zone case.

Figs. 5(a)-(b) present the deflection curves of the crown settlement δ_{cr} for no and with weak zone cases, respectively. As can be seen in Fig. 5(a) for the no weak zone case, the area between any two consecutive deflection curves, showing a maximum of 0.4%D, remains the same as the tunnel advances as reported in Steindorfer (1998). For the weak zone case shown in Fig. 5(b), however, the deflection curve ①, immediately before the tunnel heading enters the weak zone, tends to show increased crown settlements, resulting in an increased area between two neighboring deflections curves. The area between two deflection curves further increases as the tunnel heading advances deep into the weak zone. Although not shown, the deflection curves return to “normal” after the full passage of the tunnel heading through the weak zone. This trend, as previously

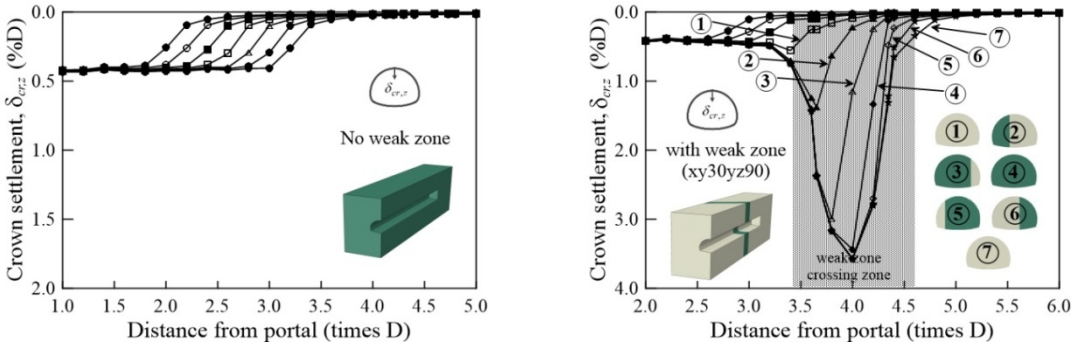

(a) No weak zone (b) xy30yz90

Fig. 5 Deflection curves: no weak zone vs. with weak zone (θ_{xy} = 30°, θ_{yz} = 90°)

suggested in a number of studies (e.g., Steindorfer 1998, Schubert *et al*. 2002, Schubert and Grossauer 2004, Grossauer *et al*. 2005, Jeon *et al*. 2005), implies that the deflection curves can give an early warning of the presence of a possible weak zone ahead of the tunnel heading.

The aforementioned studies have also shown that longitudinal displacements can vary widely when the tunnel heading approaches a weak zone in the vicinity of the tunnel, thus giving early warning for the weak zone. Fig. 6 compares the longitudinal displacement plots for no and with weak zone cases. As can be seen for the no weak zone case in Fig. 6(a), the longitudinal displacements at the crown ($\delta_{cr,y}$) and the sidewalls ($\delta_{lsp,y}$, $\delta_{rsp,y}$) are almost constant at 0.2%D during the entire tunneling process. For the weak zone case shown in Fig. 6(b), however, the longitudinal displacements significantly increase when crossing the weak zone with a sign of increase being noticed shortly before (i.e., -0.2D) the tunnel heading enters the weak zone.

A similar trend can be observed in the trend lines of displacement ratios presented in Fig. 7. As shown in Fig. 7(a), when no weak zone is present $\delta_{lsp,x}/\delta_{cr,z}$ and $\delta_{rsp,x}/\delta_{cr,z}$ remain the same at 0.8. For the weak zone case in Fig. 7(b), on the other hand, the ratios $\delta_{lsp,x}/\delta_{cr,z}$ and $\delta_{rsp,x}/\delta_{cr,z}$ start to deviate from "normal" when the tunnel heading is 0.5D away from the weak zone with their peak values occurring when the tunnel heading enters into and exits from the weak zone depending on the location of the sidewall. The sign of deviation may be "increase" or "decrease" depending on the location of the monitoring points (i.e., left or right sidewall) relative to the weak zone

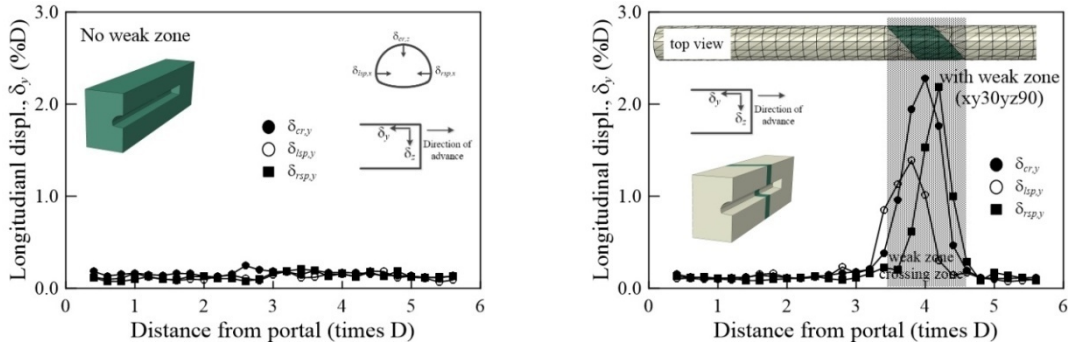

(a) No weak zone (b) xy30yz90

Fig. 6 Longitudinal displacement curves: no weak zone vs. with weak zone (θ_{xy} = 30°, θ_{yz} = 90°)

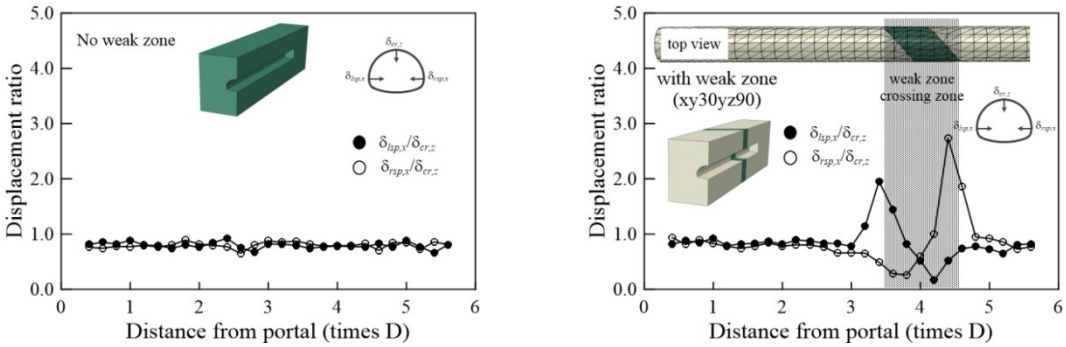

(a) No weak zone (b) xy30yz90

Fig. 7 Trend lines of displacement ratio: no weak zone vs. with weak zone (θ_{xy} = 30°, θ_{yz} = 90°)

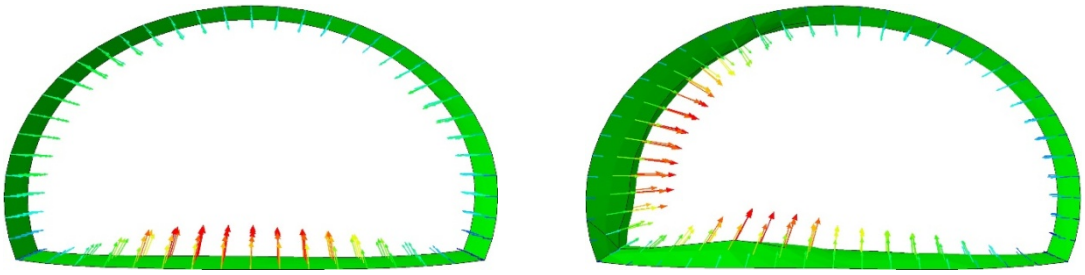

(a) -0.7D (b) -0.3D

Fig. 8 Displacement vector plots for different cross sections (θ_{xy} = 30°, θ_{yz} = 90°)

orientation. Also noted is that the deviation zone from "normal" tends to fall within the weak zone. Implications of such a trend in view of the prediction of orientation of a weak zone from the trend lines of displacement ratios will be further discussed later. According to the displacement data shown in Figs. 5~7 the detection of deviation from "normal" can be more readily made by the trend lines of displacement ratios, suggesting that the effectiveness of the aforementioned indicators depends on the orientation of the weak zone relative to the tunnel advancing direction. This will be further discussed later in this paper.

Presented in Fig. 8 are displacement vector plots for two cross sections, i.e., 0.7D and 0.3D away before the tunnel heading enters the weak zone. As can be observed in Fig. 8(a) for which the tunnel heading is at 0.7D away from the weak zone, no anomaly can be observed in the displacement vector. As the section gets closer to the weak zone, i.e., for the section 0.3D away from the weak zone, considerably increased displacements on the left sidewall of the tunnel can be observed [Fig. 8(b)]. The results shown in Fig. 8 are due primarily to the overloading of the ground between the left sidewall and the steeply dipping weak zone from the left as discussed by Steindorfer (1998).

4.2 Effect of dip angle of weak zone

The effects of dip angle θ_{yz} on the tunnel deformation behavior was examined using the results from ***Series A*** involving the cases in which a weak zone strikes perpendicular to the tunnel axis

with different dip angles.

Fig. 9 presents the deflection curves for the cases analyzed. A salient feature that can be observed in these figures is that, in all cases, an increase in the crown settlement can be recognized some distance before the tunnel heading enters into the weak zone with such a trend being more pronounced for steeply dipping weak zone cases, i.e., θ_{yz} = 90°, suggesting that early detection of weak zone using the deflection curves could be made in a more effective way when approaching steeply dipping weak zones. Fig. 10, in which the crown settlement along the path of tunnel drive is plotted against the distance to the initial appearance of the weak zone in the tunnel heading, also supports the trend shown in Fig. 9. Also observed in these figures is that the steeper the weak zone (i.e., larger θ_{yz},), the earlier the maximum crown settlement occurs when driving through the weak zone crossing zone. Furthermore, it can be noticed in Fig. 9 that the width of the zone of the increased crown settlement significantly increases with decreasing the dip angle θ_{yz} due to the wider weak zone crossing zone for the tunnel, although the maximum crown settlement $(\delta_{cr,z})_{\max}$ does not seem to significantly vary with the dip angle θ_{yz}.

The variations of the longitudinal displacement plots at the crown ($\delta_{cr,y}$) and the sidewalls ($\delta_{lsp,y}$ and $\delta_{rsp,y}$) with the dip angle θ_{yz} are shown in Fig. 11. As can be seen in these figures, the longitudinal displacement curves tend to deviate from "normal" some distance before the tunnel heading enters into the weak zone. A further examination indicates that for the gently dipping

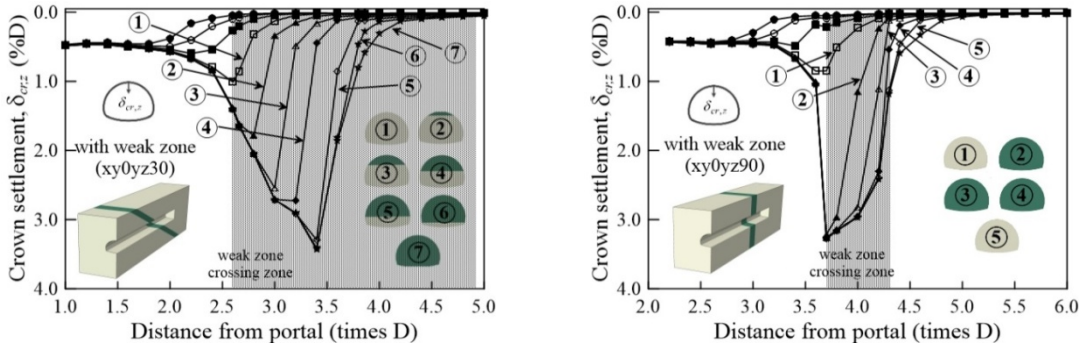

(a) θ_{yz} = 30° (b) θ_{yz} = 90°

Fig. 9 Deflection curves for various dip angles θ_{yz} (***Series A***)

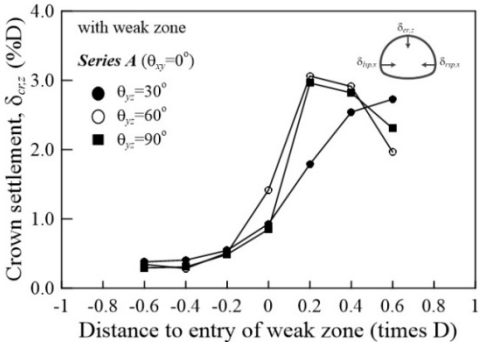

Fig. 10 Development of settlement at tunnel crown-weak zone junction for various dip angles θ_{yz} (***Series A***)

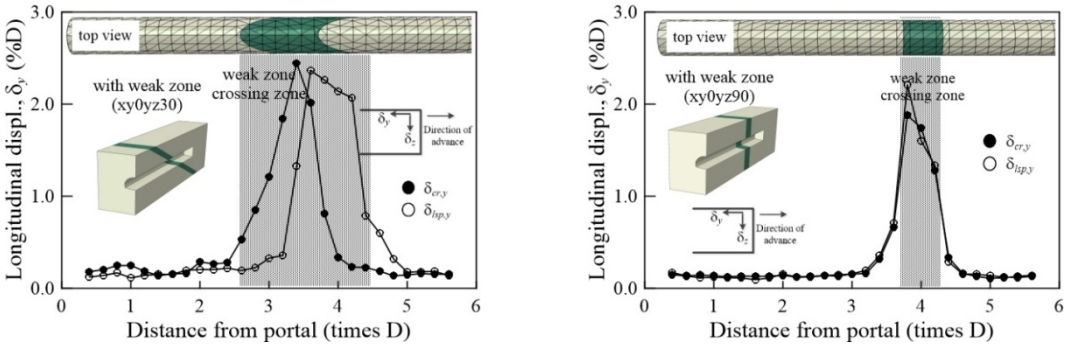

(a) θ_{yz} = 30° (b) θ_{yz} = 90°

Fig. 11 Longitudinal displacement curves for various dip angles θ_{yz} (***Series A***)

weak zone, i.e., θ_{yz} = 30°, the longitudinal displacement curve at the crown does not to deviate from "normal" until just before the tunnel heading enters the weak zone while the deviation starts much earlier for steeply dipping zone cases, i.e., θ_{yz} = 90°. Such a trend implies that for cases involving gently dipping weak zones, i.e., θ_{yz} = 30°, striking perpendicular to the tunnel axis, it would be difficult to detect the weak zone based solely on the longitudinal displacement. Another of interest trend is that the longitudinal displacement at the crown $\delta_{cr,y}$ tends to deviate earlier than that at the sidewall $\delta_{lsp,y}$, suggesting that $\delta_{cr,y}$ should be used as a primary early warning indicator over $\delta_{lsp,y}$ or $\delta_{rsp,y}$ for cases with a weak zone striking perpendicular to the tunnel axis.

Fig. 12 shows the trend lines of displacement ratios of sidewall to crown settlement, i.e., $\delta_{lsp,x}$ /$\delta_{cr,y}$ and $\delta_{rsp,x}$ /$\delta_{cr,y}$. As shown, the trend lines for θ_{yz} = 30° shown in Fig. 12(a) tend to show a sign of deviation from "normal" by decreases in displacement ratios before entering into the weak zone. The displacement ratios then increase to their peak values when excavating through the weak zone before returning to "normal" with a trend of a larger maximum displacement ratio developing for a smaller dip angle θ_{yz} (more gently dipping weak zone). It is worth noting that the trend lines for the vertically dipping weak zone case (θ_{yz} = 90°) shown in Fig. 12(b) in fact show almost a constant displacement ratio value even when crossing the weak zone, suggesting that the displacement ratios, $\delta_{lsp,x}/\delta_{cr,y}$ and $\delta_{rsp,x}$ /$\delta_{cr,y}$, would not give advance warning when crossing near vertically dipping weak zones, striking perpendicular to the tunnel axis.

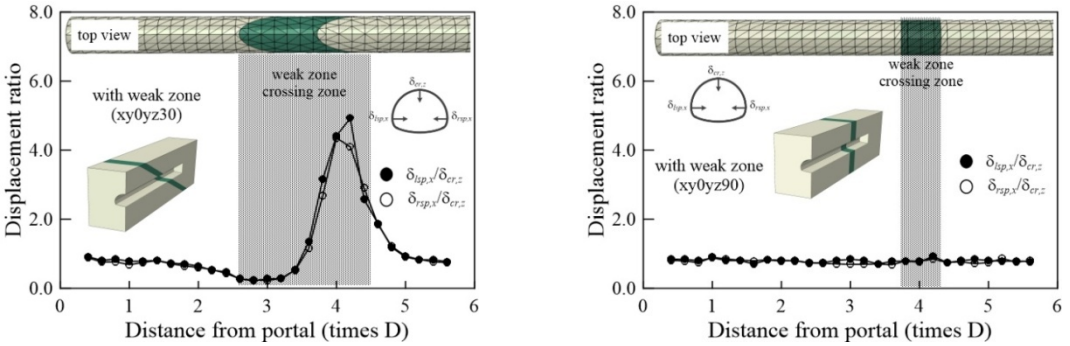

(a) θ_{yz} = 30° (b) θ_{yz} = 90°

Fig. 12 Trend lines of displacement ratio for various dip angles θ_{yz} (***Series A***)

In summary, the results presented in Figs. 9~12 for the cases with weak zones striking perpendicular to the tunnel driving axis suggest that the effectiveness of the deflection curves, the longitudinal displacement curves, and the trend lines of displacement ratios as early warning indicators is largely influenced by the orientation of the weak zone. It is therefore necessary to give full consideration to the deflection curves of crown settlement, the longitudinal displacement curves, and the trend lines of displacement ratios in relation to the orientation of the weak zone in order to detect a weak zone outside excavation area using monitored 3D displacement data. Further study is required to generalize the above findings.

4.3 Effect of strike of weak zone

The results of ***Series B*** cases are shown in Figs. 13~16, from which the effect of the strike of the weak zone relative to the tunnel axis on the tunnel deformation behavior can be identified for the vertically dipping weak zones, i.e., $\theta_{yz} = 90°$. Note that the strikes of the weak zone considered in this series of analysis include $\theta_{xy} = 0°$ and 60° measured counter clockwise from the plane perpendicular to the tunnel axis.

As can be observed in Fig. 13(a) for $\theta_{xy} = 0°$, a clear sign of crown settlement increase is noticed in the deflection curve ① for the excavation step just before the tunnel heading enters the

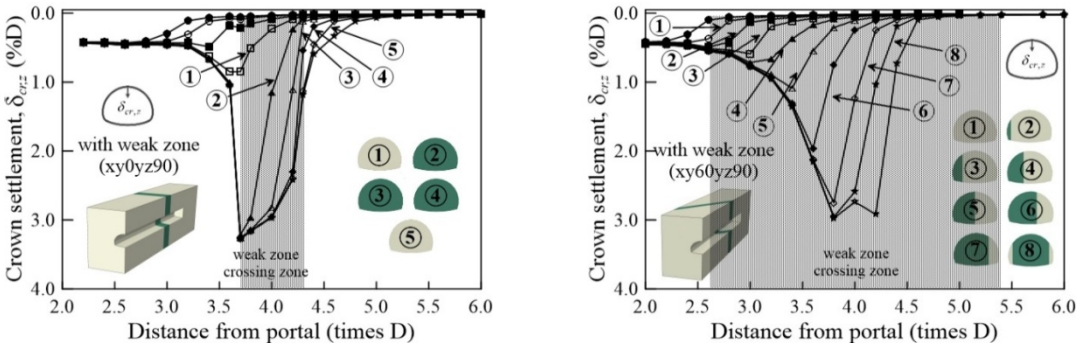

(a) $\theta_{yz} = 0°$ (b) $\theta_{yz} = 60°$

Fig. 13 Deflection curves for various strike angles θ_{xy} (***Series B*** - $\theta_{yz} = 90°$)

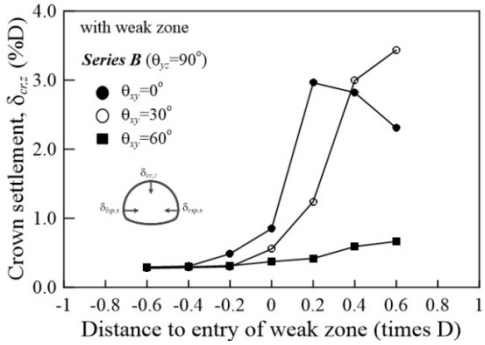

Fig. 14 Development of settlement at tunnel crown-weak zone junction for various strike angles θ_{xy} (***Series B***)

weak zone, giving early warning for the weak zone ahead of the tunnel heading. The case in which the weak zone crosses the tunnel at an acute angle, i.e., θ_{xy} = 60°, shown in Fig. 13(b), however, does not exhibit a clear sign of increase in crown settlement even when the weak zone becomes visible at the tunnel heading (see curve ②), suggesting that the deflection curve would not give early warning for a weak zone striking in an acute angle to the tunnel axis. Such a trend becomes more evident in Fig. 14, in which the development of crown settlement $\delta_{cr,z}$ in relation to the distance to weak zone entry is shown. As can be noticed, the rate at which $\delta_{cr,z}$ increases with decreasing the distance to weak zone seems greater when θ_{xy} is smaller, suggesting that the deflection curve may have better applicability as an early warning indicator when crossing weak zones striking near perpendicular to the tunnel axis.

Fig. 15 presents the longitudinal displacement plots of crown ($\theta_{cr,y}$) as well as sidewalls ($\delta_{lsp,y}$ and $\delta_{rsp,y}$). As shown, the general trend of increase in longitudinal displacements when approaching and crossing the weak zone can be observed in all cases but with different degrees in terms of early warning. For example, for the perpendicularly striking weak zone to the tunnel axis, i.e., θ_{xy} = 0°, the deviation from "normal" is noticed well before the tunnel heading enters the weak zone. For a weak zone striking in some angle, i.e., θ_{xy} = 60°, however, no apparent deviation is evident until the tunnel enters the weak zone, confirming that whether or not longitudinal displacement plots can be used as an early warning indicator strongly depends on the orientation of the weak zone. Again, the maximum values of the longitudinal displacements do not significantly vary with θ_{xy}, showing the peak values in the neighborhood of 2%D. A further examination of Fig. 15 reveals that the distribution of the longitudinal displacement curves is in accordance with the order of which each monitoring point is exposed to the weak zone. For example, for the weak zone striking perpendicular to the tunnel axis (θ_{xy} = 0°), the longitudinal displacement curves at the crown and the sidewall coincide each other. When crossing the weak zones striking to the tunnel axis in some angle towards the left sidewall, i.e., θ_{xy} = 60°, however, the longitudinal displacement curve at the left sidewall deviates first, followed by those at the crown and the right sidewall. For θ_{xy} = 60°, in fact, there exists a significant time lapse between the longitudinal displacement curves at different locations on account of the different timing of which each monitoring point is exposed to the weak zone. Such a trend suggests that the distribution of longitudinal displacement curves for different monitoring points may be used to infer the strike as well as the extent of the weak zone in relation to the tunnel driving direction.

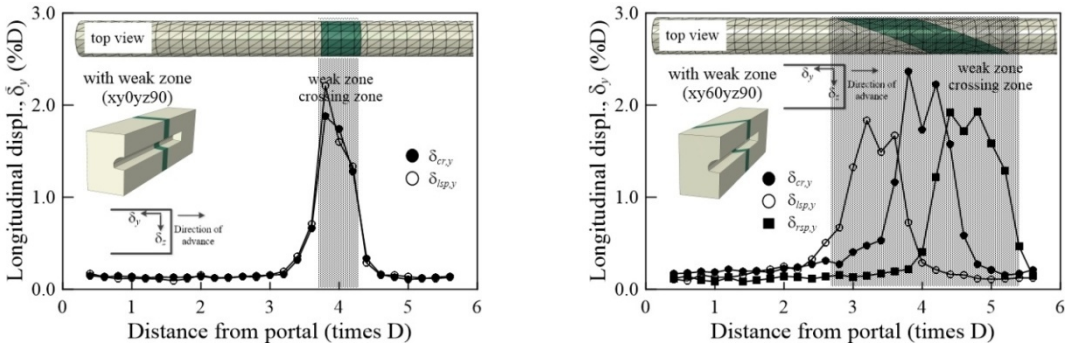

(a) θ_{xy} = 0° (b) θ_{xy} = 60°

Fig. 15 Longitudinal curves for various strike angles θ_{xy} (***Series B*** - θ_{yz} = 90°)

Presented in Fig. 16 are the trend lines of displacement ratios. Salient features are three fold. First, for the vertically dipping weak zones (θ_{yz} = 90°), the deviation of a trend line from "normal", before entering into the weak zone, becomes more evident as the strike angle to the tunnel axis θ_{yz} increases. The afore mentioned trend can be more clearly observed in Fig. 17 in which the trend lines for the left side wall are reproduced so that the time at which the tunnel heading enters into the weak zone is made the same for all cases. Second, a close inspection of Fig. 16(b) suggests that the trend lines of displacement ratios form a continuous curve with two peaks from which the width of the weak zone crossing zone (hatched area) can be inferred. Such a trend can also be observed in another sets of ***Series B*** analysis with θ_{yz} = 60°, as shown in Fig. 18. The results shown in Figs. 16~18 thus suggest that the trend lines of displacement ratios, together with the longitudinal displacement curves, may be used to identify the orientation and extent of a weak zone, for cases similar to that considered in ***Series B***. Third, unlike ***Series A***, early warning of the weak zone can be made in a more effective way using the trend lines of displacement ratios over the crown settlement and the longitudinal displacement curves. Such a trend confirms the observation made in ***Series A*** that the effectiveness of the deflection curves, longitudinal displacements, and the trend lines of displacement ratios as an early warning indicator is strongly dependent upon the orientation of the weak zone. Full consideration should therefore be given to all displacement information, rather than a single data set, to warrant early detection of a weak zone outside of the tunnel excavation area using 3D displacement data.

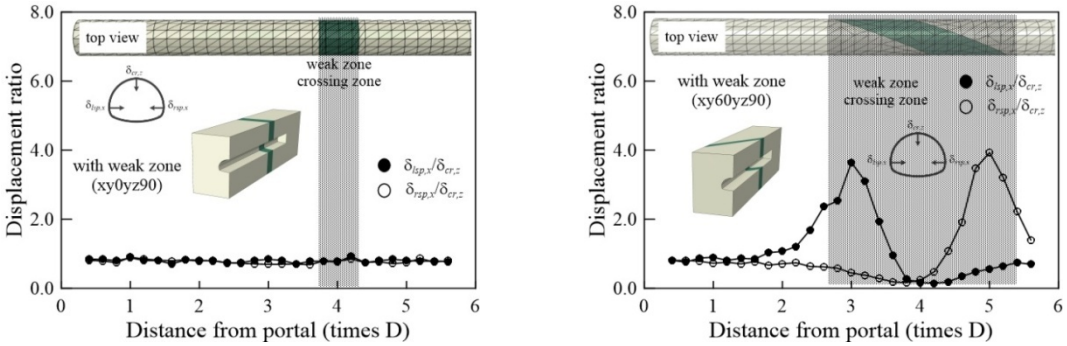

(a) θ_{xy} = 0° (b) θ_{xy} = 60°

Fig. 16 Trend lines of displacement ratio for various strike angles θ_{xy} (***Series B*** - θ_{yz} = 90°)

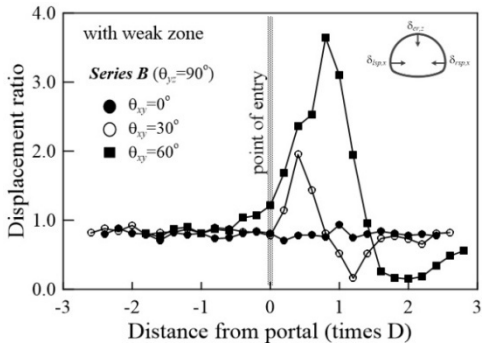

Fig. 17 Variation of trend lines of displacement ratio with strike θ_{xy} (***Series B*** - θ_{yz} = 90°)

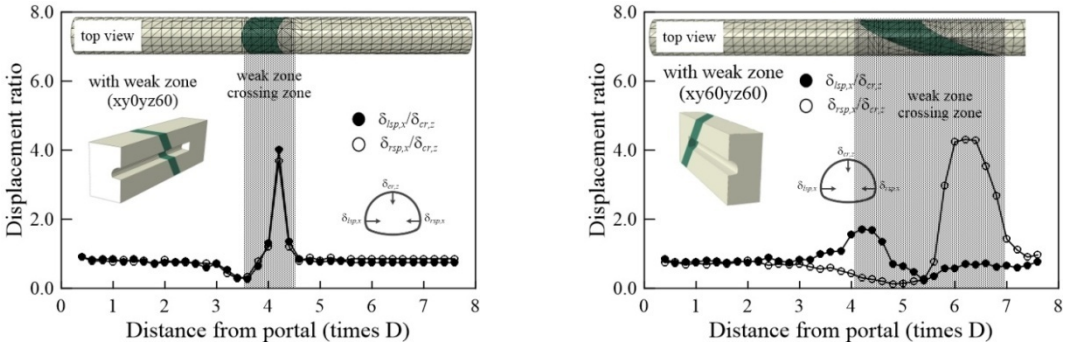

(a) θ_{xy} = 0° (b) θ_{xy} = 60°

Fig. 18 Trend lines of displacement ratio for various strike angles θ_{xy} (***Series B*** - θ_{yz} = 60°)

4.4 Effect of tunnel advancing direction with respect to dip direction of weak zone

When crossing a weak zone dipping at some angle, the tunnel drives either "with dip" or "against dip", depending on the direction of the tunnel advance with respect to the dip direction of the weak zone. The effect of tunnel advancing direction with respect to the dip direction of the weak zone was examined using the results from ***Series C***. Note here that a negative θ_{yz} represents an "against dip" case as indicated earlier. The "with dip" and "against dip" conditions were created simply by advancing the tunnel in the opposite direction using the same finite element model.

Figs. 19, 20, and 21 present the deflection curves, longitudinal displacement curves, and trend lines of displacement ratios, respectively, for the "with dip" and "against dip" cases. As can be observed, the general shapes of the curves as well as the maximum values do not significantly vary with the tunnel advancing direction. A close inspection of the deflection curves shown in Fig. 19, however, reveals that the "with dip" case tends to show the sign of deviation from "normal" much earlier than the "against dip" case. For example, for the "with dip case" (θ_{yz} = 60°) shown in Fig. 19(a), the deflection curve starts to show noticeable deviation as soon as the weak zone is slightly exposed at the upper left corner of the tunnel heading as shown in the curve ②. On the other hand, for the "against dip" case (θ_{yz} = -60°) shown in Fig. 19(b), the deflection curve ⑥ does not seem to show deviation even when a significant portion of the weak zone is exposed at the lower left portion of the tunnel heading. Such a trend is attributed to the fact that for the "against dip" case, the weak zone does not reach the crown even with which much of the lower tunnel heading is exposed to the weak zone, and suggests that deflection curves using crown settlements may not give advance warning in a timely manner when tunneling "against dip" case.

The tunnel driving direction in relation to the dip direction of the weak zone does not seem to have noticeable influence on the longitudinal displacements as no significant variation between the two cases can be observed in Fig. 20. It is, however, noted that in the "against dip" case shown in Fig. 20(b), there exists a significant time lapse for the longitudinal displacement curve at crown to show deviation after that at sidewall shows deviation when compared to the "with dip" case shown in Fig. 20(a). Such a pattern is attributed to the fact that a longer time is required for the weak zone to be exposed at the crown, after the exposure at the left sidewall, when driving "against dip".

The trend lines of displacement ratios in Fig. 21 reveal that the sign of deviation from "normal" can be noticed somewhat earlier when driving "with dip" than "against dip". Such an observation together with one made from the deflection curves in Fig. 19 suggests that early warning using the

3D monitoring data can be made more effectively for tunneling cases “with dip” than “against dip”. Another of interest trend shown in Fig. 19 is the dependency of the location of the maximum displacement ratio (left sidewall or right sidewall) on the tunnel driving direction. For example,

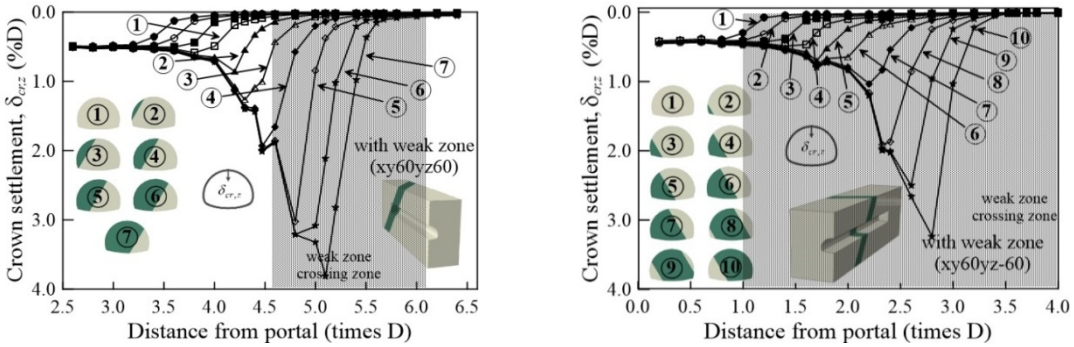

(a) With dip (θ_{yz} = 60°) (b) Against dip (θ_{yz} = -60°)

Fig. 19 Variation of deflection curves with tunnel driving direction (***Series C***)

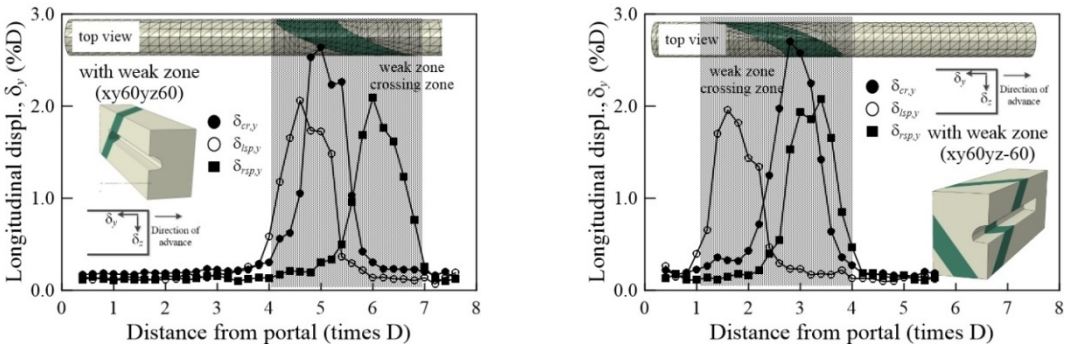

(a) With dip (θ_{yz} = 60°) (b) Against dip (θ_{yz} = -60°)

Fig. 20 Variation of longitudinal displacement curves with tunnel driving direction (***Series C***)

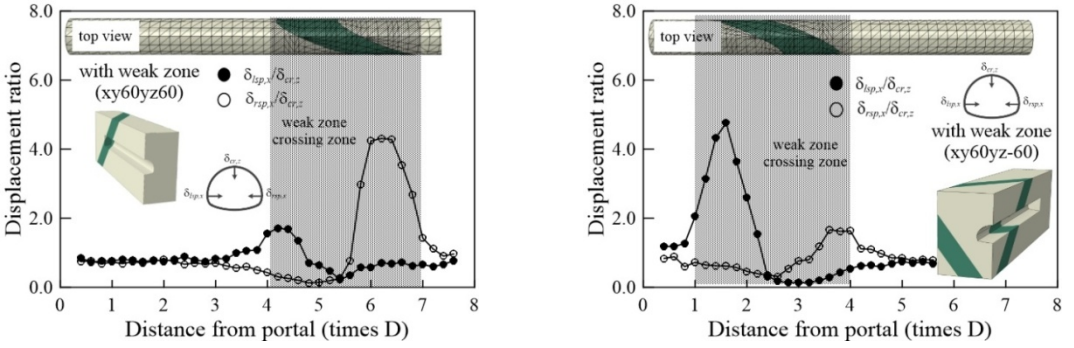

(a) With dip (θ_{yz} = 60°) (b) Against dip (θ_{yz} = -60°)

Fig. 21 Variation of trend lines of displacement ratio with tunnel driving direction (***Series C***)

when driving "with dip", the maximum displacement ratio occurs on the right sidewall whereas the opposite is true when driving "against dip". Such a trend is largely due to the spatial characteristics of the weak zone in relation to the monitoring point. In the tunneling case of "with dip", for example, the left sidewall and crown are exposed to the weak zone during an almost same excavation step while the right sidewall is exposed to the weak zone sometime after exposure of the crown to the weak zone yielding much larger displacement ratio at the right sidewall on account of small crown settlements. Again, opposite is true when driving "against dip". The pattern of trend lines of displacement ratios may therefore be used to infer information as to the direction of tunneling in relation to the dip angle.

4.5 Effect of initial stress state

Figs. 22, 23, and 24 illustrate the variations of deflection curves, longitudinal displacement curves, and trend lines of displacement ratios, respectively, with the lateral stress coefficient K_o using ***Series B*** cases. As shown, the general shapes of the displacement curves remain the same irrespective of K_o, suggesting that the early detection of the weak zone outside the excavation area using the 3D displacement monitoring data is equally valid, regardless of the initial stress state. It is, however, worth noting that early detection of the weak zone seems to be easier as the deviation

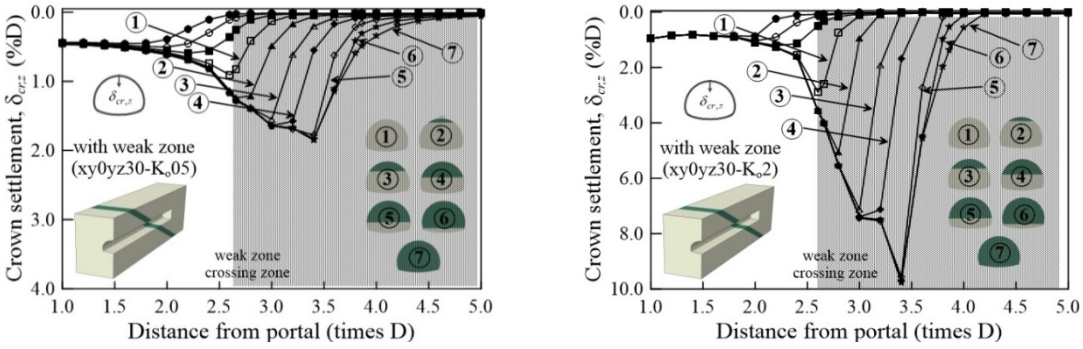

(a) K_o = 0.5 (b) K_o = 2.0

Fig. 22 Deflection curves for various K_o (***Series A*** - θ_{xy} = 0°, θ_{yz} = 30°)

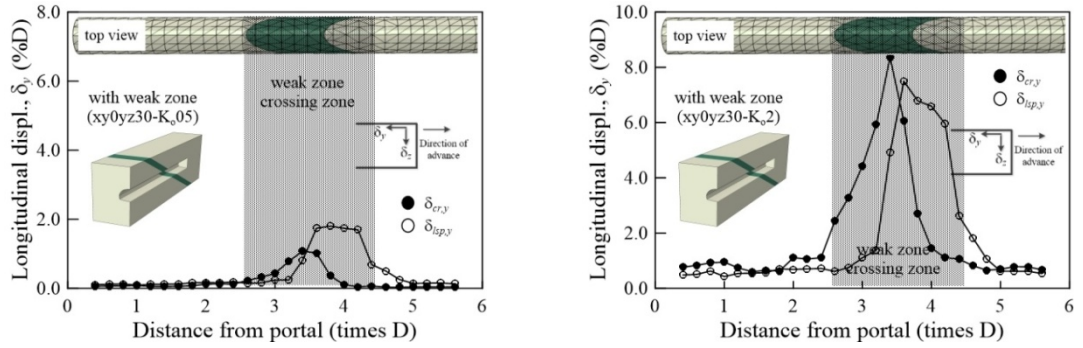

(a) K_o = 0.5 (b) K_o = 2.0

Fig. 23 Longitudinal displacement curves for various K_o (***Series A*** - θ_{xy} = 0°, θ_{yz} = 30°)

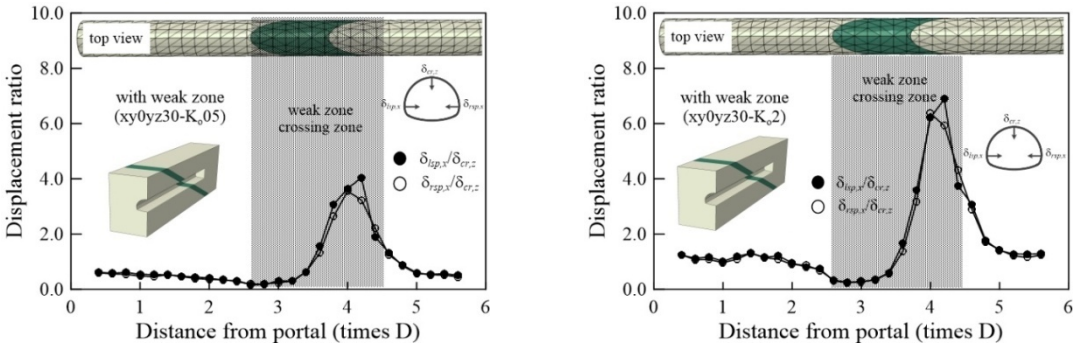

(a) K_o = 0.5 (b) K_o = 2.0

Fig. 24 Trend lines of displacement ratio for various K_o (***Series A*** - θ_{xy} = 0°, θ_{yz} = 30°)

of the displacement data from "normal" becomes more evident for a larger K_o. In addition, the maximum values in the displacement data generally tend to become greater as K_o becomes larger, although not as evident in the displacement ratios, primarily because the increasing rates of the sidewall convergence and the crown settlement with increasing K_o are similar.

5. Conclusions

In this paper, the results of a three-dimensional numerical investigation into the deformation behavior of tunnels crossing a weak zone of various orientations in conventional tunneling are presented. A series of three-dimensional finite element analyses were performed on a number of hypothetical tunneling situations, covering a wide range of spatial variations of the weak zone relative to the tunnel advancing direction together with different initial stress states. The following conclusions can be drawn from the tunneling conditions considered in this study:

(1) The results from the current study show that the shapes and extent of the deflection curve of crown settlement, the longitudinal displacement curve, and the trend line of displacement ratio are strongly related to the spatial characteristics of a weak zone outside tunnel excavation area. Although limited, it is demonstrated that the systematic interpretation of absolute displacement monitoring data allows early detection of a weak zone outside the tunnel excavation area, including the orientation of the weak zone.

(2) When approaching a weak zone striking perpendicular to tunnel driving axis, the 3D tunnel displacement indicators tend to show deviation from "normal" earlier when its dip angle is larger (steeper dip angle). Also shown is that trend lines of displacement ratio do not show any sign of deviation from "normal" when approaching and crossing a vertically dipping weak zone, suggesting that trend lines cannot be used as an early warning indicator for vertically dipping weak zones.

(3) For vertically dipping weak zones, it appears that the deflection and longitudinal displacement curves tend to give better advance warning when approaching gently striking weak zones whereas the trend line of displacement ratio gives better warning for steeply striking weak zones.

(4) The general shapes and magnitude of the crown settlement deflection curve, longitudinal

displacement curve, and trend line of displacement ratio do not significantly change with the direction of tunneling with respect to the dip direction of a given weak zone. The "with dip" case, however, tends to show better advance warning than the "against dip" case, suggesting a dependency of the effectiveness 3D displacement data for early warning on the tunnel driving direction in relation to the dip direction of a weak zone.

(5) No appreciable effect of K_o is noticed on the general shapes of the deflection curve, longitudinal displacement curve as well as the trend line of displacement ratio for the range of K_o values considered, which in turn suggests that the concept of advance warning using 3D displacement data is equally valid irrespective of K_o. The early detection of a weak zone outside the excavation area, however, seems to be easier when K_o is larger.

Acknowledgments

This research is supported by Grant No. 13CCTI-T01 from the Ministry of Land, Transport and Maritime Affairs, Korea. The financial support is gratefully acknowledged.

References

Abaqus Users Manual, Version 6.13 (2013), Hibbitt, Karlsson, and Sorensen, Inc., Pawtucket, Providence, RI, USA.

Davis, E.H. (1968), "Theories of plasticity and the failure of soil masses", Soil Mechanics: Selected Topics, Butterworth's London, UK, pp. 341-380.

Goswami, N. and Sharma, K.G. (2014), "Prediction of Ground Conditions Ahead of and Advancing Tunnel Face by Quantification of Vector Orientation", *Proceedings of Tunnelling and Underground Construction*, GSP 242, ASCE, Shanghai, China, May, pp. 216-226.

Grossauer, K., Schubert, W. and Sellner, P. (2005), "The importance of displacement prediction", *Proceedings of Underground Space Use*: *Analysis of the Past and Lessons for the Future*, pp. 1239-1244.

Incheon Airport Railway Construction Authority (IARCA) (2002), Contract 1-1 Design Report, Korea.

ITA Working Group No. 17 (2010), Repor; Long Tunnels at Great Depth.

Jeon, J.S., Martin, C.D., Chan, D.H. and Kim, J.S. (2005), "Predicting ground conditions ahead of tune tunnel face by vector orientation analysis", *Tunn*. *Undergr*. *Space Technol*., **20**(4), 344-355.

Kim, K.S., Kim, Y.S., Yoo, K.H., Park, Y.J. and Lee, D.H. (2003), "Prediction of change in ground condition ahead of tunnel face using three-dimensional convergence analysis", *Tunn*. *Undergr*. *Space Technol*., **13**(6), 476-485.

Kun, M. and Onargan, T. (2013), "Influence of the fault zone in shallow tunneling: A case study of Izmir Metro Tunnel", *Tunn*. *Undergr*. *Space Technol*., **33**(1), 34-45.

Lee, I.M., Son, Y.J. and Park, K.J. (1998), "A 3-dimensional analysis for assessing change of ground-condition ahead of the tunnel face", *J*. *Korean Civil Eng*., **18**(3-4), 505-519.

Miranda, T., Dias, D., Pinheiro, M. and Eclaircy-Caudron, S. (2015), "Methodology for real-time adaptation of tunnels support using the observational method", *Geomech*. *Eng*., *Int*. *J*., **8**(2), 153-171.

Queiroz, P.I.B., Roure, R.N. and Negro, A. (2006), "Bayesian updating of tunnel performance for K_o estimate of Santiago gravel", *Proceedings of International Symposium on Geotechnical Aspects of Underground Construction in Soft Ground*, London, UK, June, pp. 211-217.

Schubert, W. (1993), "Importance of shotcrete support in squeezing rock", *Proceedings of International Symposium*, (Fagernes, Lompen, R., Opsahl, O., Berg, K. Eds.), Lillehammer, Norway, June, pp. 277-282.

Schubert, W. and Budil, A. (1995), "The importance of longitudinal deformation in tunnel excavation", *Proceedings of the 8th ISRM Congress on Rock Mechanics*, Tokyo, Japan, September, pp. 1411-1444.

Schubert, W. and Grossauer, K. (2004), "Evaluation and interpretation of displacements in tunnels", *Proceedings of 14th International Conference on Engineering Surveying*, Zürich, Switzerland, March, pp. 1-12.

Schubert, P. and Vavrovsky, G.M. (1994), "Interpretation of monitoring results", *World Tunnelling*, 351-356.

Schubert, W., Steindorfer, A. and Button, E.A. (2002), "Displacement in tunnels – an overview", *FELSBAU*, **20**(2), 7-15.

Sellner, P.J. (2000), "Prediction of displacements in tunnelling", Ph.D. Dissertation; Graz University of Technology, Graz, Austria.

Shin, J.H., Choi, K.C., Yoon, J.U. and Shin, Y.J. (2011), "Hydraulic significance of fractured zones in subsea tunnels", *Marine Georesour. Geotechnol.*, **29**(3), 230-247.

Steindorfer, A. (1998), "Short term prediction of rock mass behaviour in tunnelling by advanced analysis of displacement monitoring data", Ph.D. Dissertation; Graz University of Technology, Graz, Austria.

Steindorfer, A. and Schubert, W. (1997), "Application of new methods of monitoring data analysis for short term prediction on tunnelling", *Proceedings of the International Symposium on Tunnels for People*, Vienna, Austria, April, pp. 65-79.

Waltham, A.C. (1994), *Foundations of engineering geology*, Blackie Academic & Professional, London.

Yang, X.L. and Yan, R.M. (2015), "Collapse mechanism for deep tunnel subjected to seepage force in layered soils", *Geomech. Eng., Int. J.*, **8**(5), 741-756.

Yoo, C. and Park, J.G. (2014), "Deformation behavior of Tunnels crossing weak zone during excavation - Numerical Investigation", *J. Korean Tunnell. Undergr. Space Assoc.*, **16**(4), 373-386.

Yoo, C., Lee, Y., Kim, S.H. and Kim, H.T. (2012), "Tunnelling-induced ground settlements in a groundwater drawdown environment – A case history", *Tunnell. Undergr. Space Technol.*, **29**(3), 69-77.

Yoo, C., Cho, Y.G. and Park, J.G. (2013), "Effect of orientation of facture zone on tunnel behavior – Numerical investigation", *J. Korean Tunnell. Undergr. Space Assoc.*, **15**(3), 253-270.

CC